



Preparation and Characterizations of PVP–TiO₂ NPs Calcined at 500, 600 and 700 °C by the Hydrothermal Method and Their Properties

J. Arul Hency Sheela¹ · S. Lakshmanan¹ · A. Manikandan² · S. Arul Antony¹

Received: 20 February 2018 / Accepted: 28 April 2018 / Published online: 4 May 2018
© Springer Science+Business Media, LLC, part of Springer Nature 2018

Abstract

The effect of the crystalline phase PVP encapsulated titanium dioxide (TiO₂) nanoparticles (NPs) to optimize the optical properties and photocatalytic activity were comparatively investigated at different calcination temperatures. The synthesized products were characterized using instrumental techniques, such as powder X-ray diffraction (XRD), Fourier-transform infrared spectroscopy (FT-IR), transmission electron microscope, energy dispersive X-ray, ultraviolet–visible (UV–visible), photoluminescence (PL) and vibrating sample magnetometer. The functional groups were identified by the FT-IR analyses. XRD result showed that the anatase and rutile phase structure of TiO₂ NPs was confirmed. The spherical shaped morphology is predicted by the SEM analysis. The optical properties of the TiO₂ NPs were studied by the UV–visible and PL analysis. The magnetic behavior of the TiO₂ NPs was studied. Photocatalytic activity of TiO₂ NPs was tested by the degradation of MeB dye under UV light irradiation. In addition, the chemical oxygen demand removal follows the photo degradation in behaviour was observed.

Keywords PVP–TiO₂ · Hydrothermal · 500, 600 And 700 °C · Optical · Magnetic · Photocatalytic

1 Introduction

Metal oxide nanoparticles were successfully prepared by the several methods and it is much more attention because of these nanoparticles has unique electrical, optical and magnetic properties, which are different from their bulk counterparts. The metal oxide NPs have best potential applications for different industrial fields because of their tremendous properties in high hardness, high thermal conductivity, low melting point, low density, high thermal conductivity [1–3]. TiO₂ has attracted much more interest as an optoelectronic material for numerous applications with a direct band gap of 3.2 eV and it is used as type of semiconductor catalyst for the degradation of water pollutants. TiO₂ is the most exhaustively investigated transition metal oxide with depend on their physical and chemical process and it offers promising candidature for potential applications such as, solar thermal

absorber, catalyst for oxygen evolution, electro chromic device and photo electrolysis [4–6]. There are several factors in determining important properties in the performance of TiO₂ NPs for applications such as size, crystallinity, shape and morphology [7–9].

- (i) Physical methods: thermal evaporation, CVD, ball milling, molecular epitaxial and etc. that methods have requires to high vacuum and energy consuming [10–15].
- (ii) Chemical methods: wet-chemical, reflux, sol–gel, solvothermal, hydrothermal and etc. among them the hydrothermal has a low cost, easy manipulation, room temperature, high dispersion and etc. and also emerged because of useful for new applications in materials science in UV and gas sensor, UV-photo detector, lithium batteries and optoelectronics devices [16–19].

✉ S. Arul Antony
lachuchem666@gmail.com

¹ Department of Chemistry, Presidency College
(Autonomous), Chennai 600 005, India

² Department of Chemistry, BIHER, Bharath University,
Chennai 600 073, India

TiO₂ NPs was successfully prepared via hydrothermal method in terms on the size, shape, morphology, optical and photocatalytic activity. PVP–TiO₂ NPs imparts useful characteristics to the material for specific applications and it attracted great attention because of the combination of

interesting properties [20, 21]. Semiconductors (TiO_2) NP depend on their crystallite size, making clusters and stabilized using various polymers as surfactants due to their high surface to volume ratio in high chemical reactivity. PVP acts as a stabilizer, water soluble polymer, capping molecules through the electrostatic and steric stabilization of the amide groups, this due to dissolved metallic salts. Hydrophilic and hydrophobic acted as the head and tail group from the PVP process [22, 23]. The chemical reaction of the PVP has two types is given below.

- (i) Growth of the TiO_2 particles was controlled via forming passivation layers by the coordination bond between the Ti^{4+} ions and nitrogen atom of the PVP [24].
- (ii) Due to the repulsive force acting among the polyvinyl groups by the steric effect [25].

PVP is non-ionic surfactant used for capping agent prevent them from agglomeration and improve the interaction between IV and VI group semiconductors and PVP based on Density Functional theory (DFT) was studied. It is used to clarify the mechanism of interaction of metal sulfide with PVP polymeric matrix understanding the mechanism of adsorption of pyrrolidinone on the surface of metal oxide NPs. PVP on the IV–VI group semiconductors particle surface was attraction among their polymeric chains due to the osmotic pressure, which causes destabilization and it is known as depletion flocculation. IV–VI group semiconductors have a wide utilization in numerous applications, such as optoelectronic, photothermal, and LED because of their huge direct bandgap [26, 27]. Among them, the preparation of semiconductor nanoparticles (TiO_2) by the hydrothermal method is easily aggregated and thus loses their activity. Above lose are rectified to preparation of TiO_2 nanoparticles, which is used for PVP act as a capping agent to provide chemical passivation that prevent from agglomeration and improve the surface states and stability. PVP has a many advantages in simple procedure, transparency in the UV light and easily available in society. The TiO_2 to diffuse in water and make effective contact with dye molecules from photocatalytic process, this was due to the polymer shells allow the catalytic nanoparticles and polymer (PVP) are dispersible in water and could form stable suspension [28, 29]. PVP plays an important role on the particles surface to transfer the photo generated electrons and holes and it can be also minimized by dispersing over the surface of a polymeric support at the nanosize particles. In this work, in order to improve prior achievements, we try to give deeper view of the PVP function that affords the enhanced photo activity and photocatalytic performance. In the present paper, there is no report on the synthesis of PVP– TiO_2 NPs obtained by simple hydrothermal process in terms on their structural,

morphological, optical, magnetic and photocatalytic activity were comparatively investigated. In addition, the high photocatalytic activity of PVP– TiO_2 NPs was evaluated using the degradation MeB under UV light with compared to Degussa P-25.

2 Experimental Procedure

2.1 Materials

All the chemical reagents were commercial with AR purity and used directly without further purification. In compound, Titanium Tetraisopropoxide (TTIP), Potassium nitrate (KNO_3), Polyvinylpyrrolidone (PVP), Nitric acid (HNO_3) and Distilled Water, were purchased from Merk and Sigma-Aldrich in India (Tamil Nadu). The Methylene blue (MeB) stock solution with concentration of 3.26×10^{-4} mol/L was prepared by the dissolving MeB liquid in de-ionized water.

2.2 Preparation of PVP– TiO_2 NPs

Present work, 3.25 g of cationic precursor (TTIP) and 2.12 g of anionic precursor (KNO_3) was dissolved in 80 mL of distilled water. In addition 0.5 g of PVP was added. Then, a few drops of HNO_3 were added to adjust the pH as well as restrain the hydrolysis process under stirring for 2 h. The above mixed solution was transferred into a 100 mL Teflon-lined stainless autoclave and maintained at 180 °C for 2 h at a ramping rate of 5° min^{-1} . Then, obtained powder was obtained and calcined at 500 °C for 3 h. The similar procedure was followed for the preparation of PVP– TiO_2 calcined at 600 and 700 °C.

2.3 Characterization Techniques

The functional groups were identified by the FTIR spectra (Nicolet 305 spectrometer). The phase transformation of PVP– TiO_2 were characterized by the powder XRD, XPERT PRO with $\text{CuK}\alpha$ X-ray radiation ($\lambda = 0.15496$ nm). The spherical-like morphologies were carried out by the HR-SEM JOEL-JEM-2010 studies. The high magnification images were observed by the TEM (Philips model CM 20) analysis. The absorption study of the PVP– TiO_2 has been carried out by the Varian Cary 5E UV–vis spectrophotometer. The PL spectra of the TiO_2 NPs were studied by the Fluoromax 4 spectrofluorometer, with a Xe lamp as the excitation light source. The magnetic behavior of the PVP– TiO_2 NPs was carried out in a Vibrating Sample Magnetometer model at VSM-EG and G PARC VSM 155. UV–visible spectrum of the PVP– TiO_2 were observed using Perkin Elmer UV–visible spectrometer RX-1. Photocatalytic experimental was fixed in a 600 mL cylindrical vessel

with an 8 W Mercury Vapour lamp was installed in a quart glass tube to protect it from direct contact with the aqueous solution. 50 mg of the photocatalyst were added into the 100 mL of MeB dye solution. Above reaction suspensions was sonicated for 20 min and magnetically stirred in a dark condition. The resultant initial concentration of the MeB dye solution was calculated to be 4.3×10^{-4} mol L⁻¹. Obtained ZnS samples of 2 mL volume were withdrawn from the suspensions for every 20 min from the MeB dye solution using a centrifuge, which was transferred back to the original solution mixture. The concentration of the MeB dye solution was analyzed by the UV–visible spectrometry. PVP–TiO₂ NPs was refluxed with HgSO₄, AgSO₄, H₂SO₄ with a known volume of standard K₂Cr₂O₇ for 2 h. The above solution was titrated with standard FAS using ferroin as indicator and COD was determined. A blank titration was observed using de-ionized water instead of MeB dye [8, 9, 17].

$$\text{COD} = (\text{Blank titrate value} - \text{MeB dye sample titrate value}) \times (\text{normality of FAS} \times 8000) \times (\text{Volume of sample})^{-1}$$

3 Results and Discussion

3.1 FTIR Analysis

FT-IR spectra of the TiO₂ NP dried at 120 °C as shown in Fig. 1. The broad absorption band was observed at around ~ 3405 cm⁻¹, this was due to existence of the stretching vibration at hydroxyl groups on the TiO₂ NP surfaces. Since, the small peak was observed at around ~ 1642 cm⁻¹, this was due to bending vibration of adsorbed water molecules and the weak band was located at around ~ 1451 cm⁻¹, it

can be assigned to the stretching vibration of the C–H bond, this was due to presence of some organic molecules on the TiO₂ NPs surfaces [30, 31]. Moreover, the strong absorption bands were observed at around ~ 821 and ~ 566 cm⁻¹ and it can be attributed to the Ti–O–Ti stretching mode of vibration.

3.2 XRD Analysis

XRD patterns of the TiO₂ NPs calcined at 500, 600 and 700 °C as shown in Fig. 2a–c. The observed diffracted peaks were indexed to the tetragonal anatase phase, which is in good agreement with standard data (JCPDS No. 21-1272) [32, 33]. No extra peaks were observed due to the high purity of the obtained products. The average crystallite sizes of the PVP–TiO₂ NPs are found to be $\sim (24\text{--}35)$, $\sim (42\text{--}58)$, $\sim (65\text{--}88)$ nm using Scherrer's formula and it is

clearly seen that the crystallite size is increased as well as increasing temperature. Figure 1a, b shows the high degree of crystallinity and the existence of anatase phase TiO₂ NPs calcined at 400 and 500 °C, which is increased calcination temperature at 700 °C leads to the formation of rutile phases. In addition, the anatase phase was disappeared completely, when the calcination temperature was increased at 700 °C. TiO₂ NPs a great extend of the phase transformation as anatase to rutile due to increasing temperature [34, 35]. XRD result that the anatase phase was stabilized at 400 and 500 °C, but the transition to the rutile phase was suppressed on increasing calcination temperature at 700 °C.

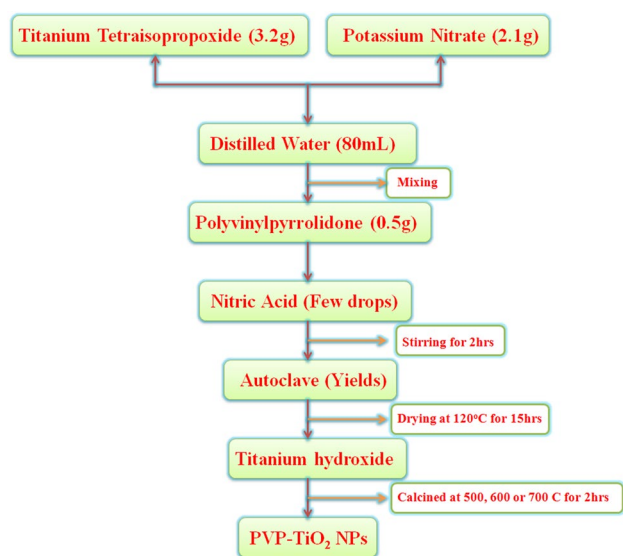


Fig. 1 Shows the flow chart diagram of PVP–TiO₂ NPs

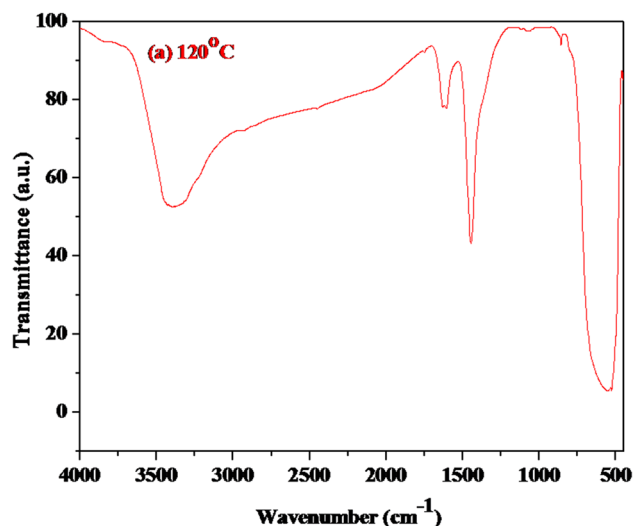


Fig. 2 Shows the FT-IR spectrum of TiO₂ NPs dried at 120 °C

3.3 SEM–EDX Analysis

SEM–EDX images of the TiO₂ NPs calcined at 500, 600 and 700 °C as shown in Fig. 3a–c. The spherical-like morphology was predicted for all three TiO₂ samples. It is clearly seen that the TiO₂ particles calcined at 500 °C shows well-defined homogeneous spherical-like particles than the TiO₂ particles calcined at 600 and 700 °C [22]. From EDX images, the compositional elements of the obtained products were confirmed such as, titanium and oxygen [36, 37].

Figure 4 shows the possible formation mechanism of the PVP–TiO₂ NPs is proposed. PVP also serves as template to induce the hierarchical structures, as titanium hydroxide presents microstructures. The carbonyl oxygen of PVP can form coordinative bonds with Ti⁴⁺, which is illustrated by FT-IR analysis. It is found that the CO band of PVP shifts from 1648 to 1640 cm⁻¹ after adding TTIP, indicating the coordination interactions between Ti⁴⁺ ions and the carbonyl group [38]. A new band at 1642 cm⁻¹ appears in the FTIR spectrum that is thought to be associated with the weak interactions

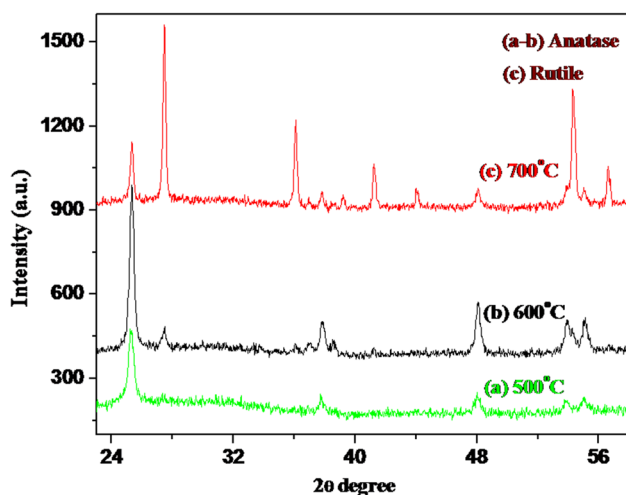


Fig. 3 a–c Shows the XRD of TiO₂ NPs at 500, 600 and 700 °C

between the Ti⁴⁺ ions and the carbonyl groups of PVP. Furthermore, it is found that PVP could be selectively adsorbed on the species crystal plane. In the hydrothermal process, due to the intrinsic tetragonal layer-structure and selective adsorption of surfactant PVP molecules on the crystal faces, TiO₂ crystal nuclei anisotropically grow into spherical when the amount of PVP is small in the reaction; the obtained TiO₂ presents spherical structures in nanoscale regime. The reason is that the limited amount of PVP only acts as the carbon and oxygen source to form TiO₂, and not enough PVP serves as the so template to induce the spherical-assembly in nanoscale [39]. With the increased calcination temperature amount of PVP, these nano spherical can assemble into a hierarchical agglomeration through molecular interaction between surfactant molecules as well as increased particle size by the minimization of surface energy. Apart from the important role of PVP, it is interesting to additive affects the growth process. It has been reported that a wide range of additive substances have been made available to steer the assembly of structural building blocks into a defined morphology on the nanoscale as an alternative control approach. In the present work, the addition of PVP greatly increases the ionic strength of the growth solution, which favours the formation of smaller crystals through electrostatic screening. Therefore, the time dependent experiments demonstrate the microspheres are gradually assembled by spherical structure with the increase calcination temperature. The generation of TiO₂ may be attributed to the partial substitution, which may be attributed to the rutile and anatase structure of TiO₂ [40].

3.4 TEM–SAED Patterns Analysis

TEM–SAED patterns of the TiO₂ NPs calcined at 500, 600 and 700 °C as shown in Fig. 5a–c. TiO₂ particles appeared in the aggregated, agglomerated and fine-spherical shaped smaller particles [40, 41]. The particle size of the TiO₂ NPs are estimated to be ~ (19–25), ~ (34–48), ~ (51–72) nm, respectively. From SAED pattern (insert Fig. 5a), the obtained rings are assigned to the reflections of the anatase

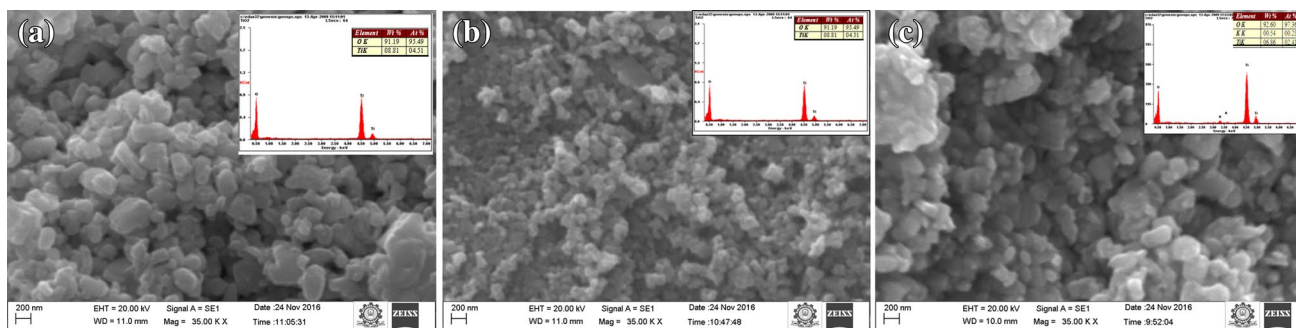


Fig. 4 a–c Shows the TEM–SAED of TiO₂ NPs at 500, 600 and 700 °C

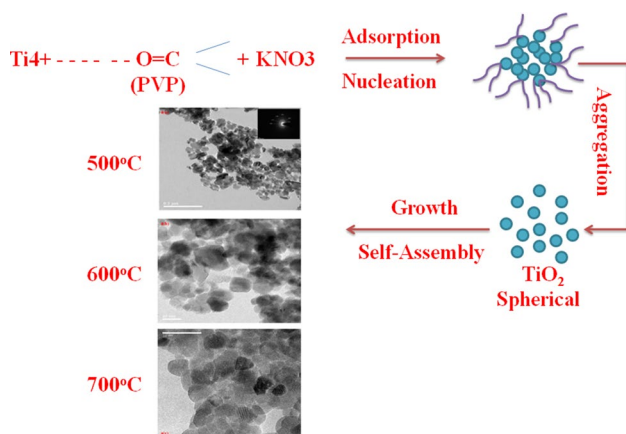


Fig. 5 a–c Shows the SEM-EDX of TiO₂ NPs at 500, 600 and 700 °C

phase, which is in good agreement with the XRD results. In addition, the diffraction rings are exhibited that the good crystallinity and size of the smaller particles [41].

3.5 UV Analysis

Absorption spectra of the TiO₂ NPs calcined at 500, 600 and 700 °C as shown in Fig. 6a–c. The strong absorption edge was observed in UV region at 325, 338 and 346 nm. An obtained product indicates that the blue-shifted towards the shorter wavelength and it clearly shows the uniform distribution of particle size than the bulk counterparts (TiO₂). Moreover, the absorption edge can be shifted to the higher energy, when the particle size decreases due to quantum confinement effect [41, 42]. The direct bandgap energies of the TiO₂ NPs are found to be 3.68, 3.53 and 3.25 eV, which is higher compared to bulk counterparts (TiO₂) by using the direct transition equation for photon energy versus $(\alpha h\nu)^2$ [$(\alpha h\nu)^2 = A(h\nu - E_g)$]. Where, α is an absorption coefficient, A is the constant, E_g is the Band gap and the extrapolation of the linear portions of the curve towards the absorption equal to zero gives E_g for the direct transitions [42].

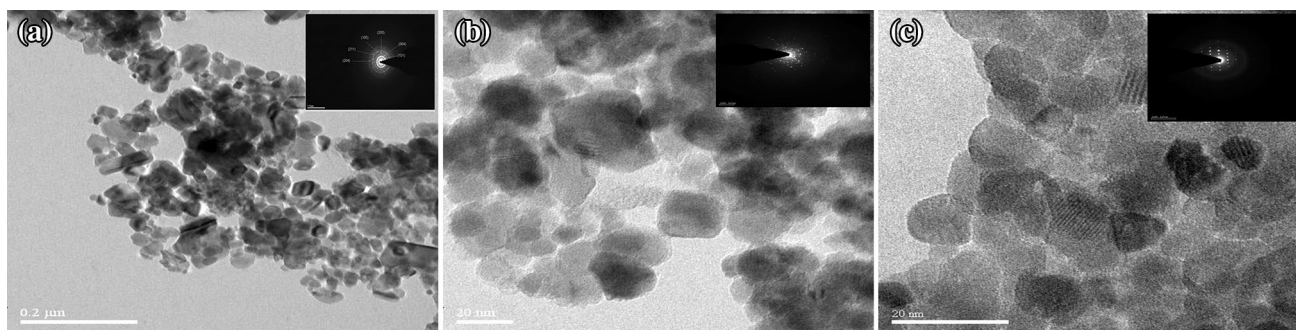


Fig. 6 Shows the growth mechanism for the formation of PVP-TiO₂ NPs

3.6 PL Analysis

PL spectra of the TiO₂ NPs calcined at 500, 600 and 700 °C as shown in Fig. 4a–c. The emission spectra were observed in UV region at 348 nm with an excitation wavelength of 325 nm. The UV emission originated from an excitonic recombination can be attributed to the surface a defect corresponds to the near-band-edge emission of TiO₂ NPs [42, 43]. The high UV emission indicates a good crystal quality and low density of surface defects of the obtained products, that there is change in the broadening of the emission peaks by the increase of calcinations temperature, which indicates that the uniform particle size and increased surface defects and it is used for optoelectronic devices in nanoscale region [43].

3.7 Magnetic Behavior

Magnetic behavior of the PVP-TiO₂ NPs calcined at 500 °C as shown in Fig. 7. It is clearly seen that the magnetization values are increases rapidly at lower fields, which is indicates their ferromagnetic behavior. The saturated magnetizations (M_s) for the PVP-TiO₂ NPs are found to be 0.19 emu/g and coercive forces (H_c) is 129 Oe. Therefore, obtained ferromagnetism in the PVP-TiO₂ NPs was confined to the surface of the NPs, which is due to oxygen vacancies with strong magnetization at room temperature and it is used for spintronic devices applications [43–45].

3.8 Photocatalytic Activity

Photocatalytic of the PVP-TiO₂ NPs calcined at 500 and 700 °C using MeB dye. The characteristic absorption of methyl orange at 650 nm and it is a well known acid-base indicator. Herewith, the obtained samples were collected at various time intervals. The decreased absorption intensity indicated that the PVP-TiO₂ catalyst products to degrade with respect to the irradiation time that indicate strongly active in the degradation of the catalytic process corresponds

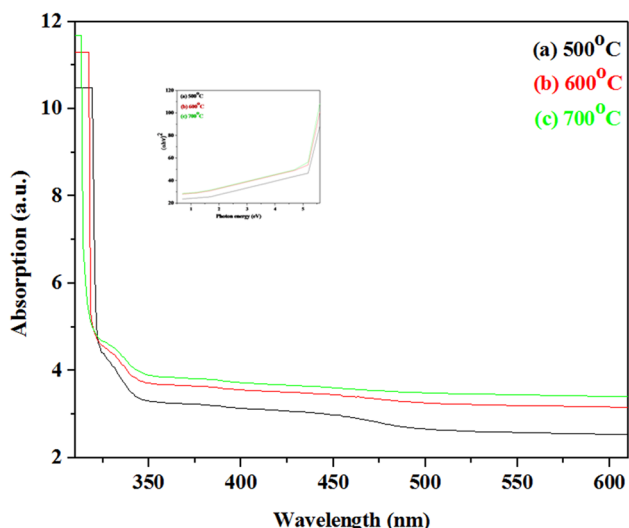


Fig. 7 a–c Shows the UV–Visible of TiO₂ NPs at 500, 600 and 700 °C

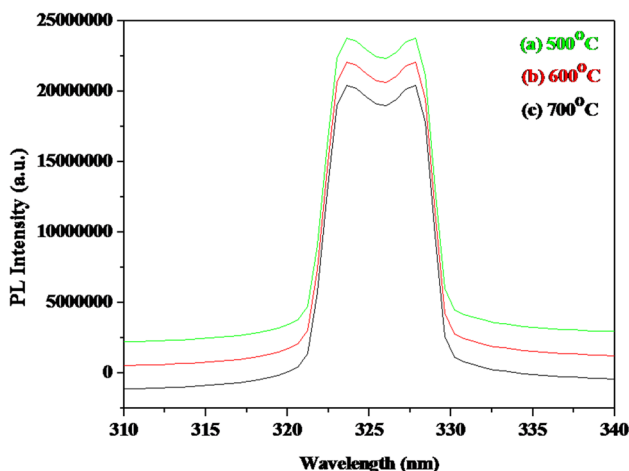


Fig. 8 a–c Shows the PL of TiO₂ NPs at 500, 600 and 700 °C

to the molecule decreased, this was due to the concentration of the MeB dye decrease with irradiation time increase. No new absorption peaks are present in the UV or visible region. The use of the sample P-25 is chosen as a reference to our investigation of PVP–TiO₂ NPs. Hence, study of the degradation process was confirmed from the semiconductor (TiO₂) materials, which indicate the complete photo degradation of MeB dye [45]. Degradation efficiency of the absence and presence in the PVP–TiO₂ NPs calcined at 500 and 700 °C using MeB dye as shown in Fig. 8a–c with compared to Degussa P-25. Degradation efficiency (η) formula is $\eta = \frac{C_0 - C_t}{C_0} \times 100\%$ with the C_0 -before illumination and C_t -after irradiation at a time (t) and it is degradation percentage of the MeB dye is found to be 91 and 78% for the

obtained products. Table 1 shows the degradation data of the absence and presence of PVP–TiO₂ NPs [4–6, 46]. The blank test reaction rate constant was calculated to be 0.20×10^{-3} . The PVP–TiO₂ NPs calcined at 700 °C is found to be 1.86×10^{-3} and $3.26 \times 10^{-3} \text{ min}^{-1}$. Similarly, PVP–TiO₂ NPs calcined at 500 °C is found to be 2.15×10^{-3} and $6.24 \times 10^{-3} \text{ min}^{-1}$. The above result shows that the low calcination of PVP–TiO₂ NPs has strong degradation efficiency than the high calcination of PVP–TiO₂ NPs, this was due to photon absorption on the PVP–TiO₂ catalyst surface and high surface to volume ratio.

Table 2 gives the COD values of initial and final treated PVP–TiO₂ NPs indicate the almost complete mineralization of the MeB dye. To measure the organic contaminants strength of wastewater, an effective technique is to measure the total quantity of O₂ required for the oxidation of organic compound to CO₂ and H₂O using COD test applying K₂Cr₂O₇ method. The degradation was obtained that confirms the mineralization of MeB dye by using COD values. Although TiO₂ Degussa P-25 has the highest catalytic activity for MeB disappearance and it is clearly appearance that the PVP–TiO₂ (500 °C) has been important efficiency in their total mineralization in UV light irradiation. Since, the total degradation involves many consecutive reactions before reaching CO₂. This is underlining the interest of using TiO₂ catalyst to decontaminant wastewater [46, 47]. The COD values decrease in the degradation process indicating that the high potential of the low calcination of PVP–TiO₂ catalyst high calcination of PVP–TiO₂ catalyst.

Figure 9a–c shows the TOC (mg L⁻¹) versus various irradiation time intervals in the absence and presence PVP–TiO₂ catalyst with compared to Degussa P-25. TOC concentration of MeB dye solution involved in various reaction times was observed in the PVP–TiO₂ catalyst. MeB dye solution was effectively mineralized to CO₂ and H₂O. It is clearly seen that the absence of MeB dye solution has lesser mineralization than the presence of PVP–TiO₂ NPs. The total organic carbon disappearance which is follows apparent first order kinetic with a conversion in CO₂ of 91%. The fastest and most easily eliminated TOC is that of PVP–TiO₂ (500 °C). Both parameters as COD and TOC, which are directly, evaluate the pollution level of a aqueous solution do not exhibit similar disappearance patterns. This is could be accounted for by the influence of the PVP and various calcination temperatures on their reactivates with ·OH radicals and the photo catalysis of ·OH radicals is considered to be the most efficient species [11, 47]. From the toxicological point of view, the TOC analysis seems more accurate and appropriate for evaluating the determination of polluted water containing organics. The above TOC results show that the low calcinations of PVP–TiO₂ have strong photocatalytic activity [48].

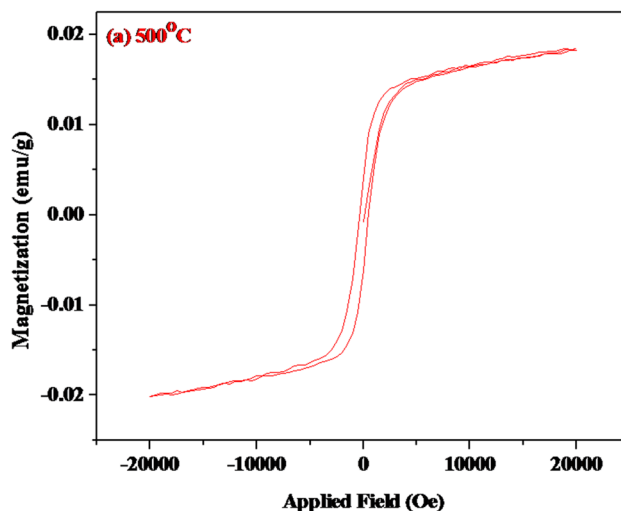
Figure 10 shows the schematic diagram of photocatalytic process for the PVP–TiO₂ catalyst using MeB dye.

Table 1 Shows the photo degradation data of the absence and presence of PVP–TiO₂ NPs

Sample	Mixtures of PVP–TiO ₂ surface		700 °C (%)	500 °C (%)	700 °C (%)	Degradation efficiency (%)	Reaction rate constant after 120 min (min ⁻¹) × 10 ⁻³
	500 °C	700 °C					
	Blank						
1	Blank		0	0	0	19	0.19
2	1	0	100	0	42	76	2.15
3	2	1	71	28	51	71	3.25
4	2	1	62	36	62	60	4.13
5	1	2	44	58	75	49	5.11
6	1	2	32	77	84	37	5.64
7	0	1	0	100	91	28	6.26

Table 2 Gives the COD values of initial and final treated PVP–TiO₂ NPs

Concentration of MeB dye (10 ⁻⁵ M)	Initial COD (mg L ⁻¹)	Final COD (mg/L) PVP–TiO ₂		Photo degradation efficiency (%) PVP–TiO ₂	
		500 °C	700 °C	500 °C	700 °C
		1	9.17	17.71	21.22
2	89.42	8.82	12.51	45.32	37.33
3	226.35	26.21	36.52	59.21	48.25
4	396.41	29.28	59.12	75.21	59.35
5	451.14	32.33	67.74	83.35	70.21
6	596.73	38.87	79.21	90.75	78.22

**Fig. 9** Shows the VSM of TiO₂ NPs at 500 °C

Degradation of the photocatalytic process was generated by the hole (h⁺) and electron (e⁻) pair using MeB dye. PVP–TiO₂ catalyst is illuminated by the UV light and enhanced energy is equal or greater than the bandgap energy of the bulk counterparts. The electrons are excited from the valence band to the conduction band, which releases hole in the valence band due to the process of photo excitation in semiconductor materials as shown in Fig. 10. It shows the induced electrons and holes are transferred separately to the surface of the PVP–TiO₂ catalyst react with the O₂, OH⁻ involved in the MeB dye solution lead to the formation of superoxide radical anions (O₂⁻) or hydroxyl radicals (·OH). The photocatalyst surface was converted from the adsorbed oxygen to the formation of the super oxide radical (O₂⁻) and the reaction of the valence band hole (h⁺_{VB}) with adsorbed HO⁻ ions lead to the formation of ·HO radicals that reveal that the neutralization of the super oxide radical (O₂⁻) and it lead to the formation of hydrogen peroxide with the cleavage of H₂O₂ to form HO. Radicals [49, 50].

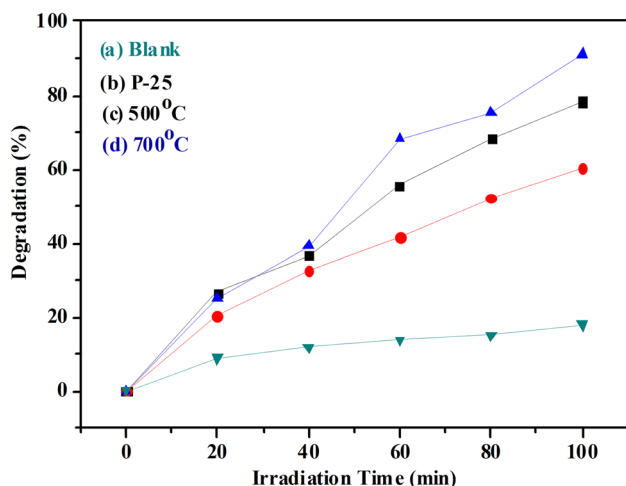
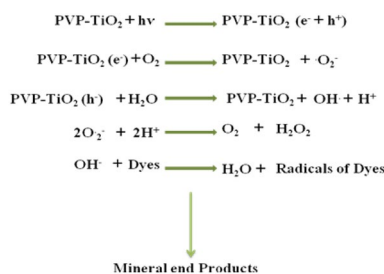


Fig. 10 *a–d* Shows the degradation (%) of TiO₂ NPs at 500 and 700 °C

The degradation of the substrate of the h⁺ or HO radical and various reaction involved in the degradation of PVP–TiO₂ catalyst is given.



3.9 BET Surface Area and Porosity

Figure 11a–b shows the pore size distribution curve (inset) of PVP–TiO₂ NPs was characterized by the N₂ adsorption–desorption isotherms. The obtained product has isotherms that possess some features of semiconductor materials and it exhibits a relatively low adsorption at high relative pressures as suggesting the presence of some micropores in below 0.3. The isotherm curve has a hysteresis loop characteristic of IV isotherms at low relative pressures in above 0.25, this was indicating that the obtained product has presence of micropores. Therefore, the adsorption branch increases rapidly at relative pressures close to unity that characteristic of the type II isotherms [50, 51]. The surface area and pore volume of the obtaining product was found to be at 225 and 210 m² g⁻¹ (500 °C) and 0.54 and 0.45 cm³ g⁻¹ (500 °C) corresponding pore size distribution indicates a wide distribution range at ~ (19–25) and ~ (51–72) nm for 500 and 700 °C PVP–TiO₂ NPs. The above

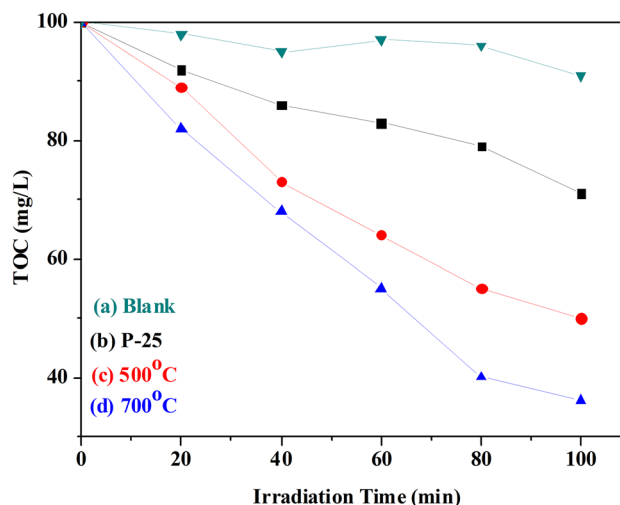


Fig. 11 *a–d* Shows the irradiation time TiO₂ NPs at 500 and 700 °C

porous structure is extremely useful in catalyst as they will provide efficient transport pathways to reactant molecules and mineral products (Figs. 12, 13). The obtained product may be embedded within pores present in the shells of these TiO₂ particles causes a small reduction in the specific surface area. The BET results showed that the shell of TiO₂ particles was composed of many fine crystallites and had a micro porous structure demonstrated by N₂ adsorption/desorption isotherm [52].

4 Conclusion

PVP–TiO₂ NPs were successfully prepared through a simple hydrothermal method under various calcination temperatures was investigated and affects the crystal structure, particle size, morphologies and photocatalytic activity. The phase transition of the PVP–TiO₂ NPs were observed such as, anatase to rutile, this was due to calcination temperatures. The above synthesis process is time and energy saving, that will be useful in low cost of the PVP–TiO₂ catalyst. The

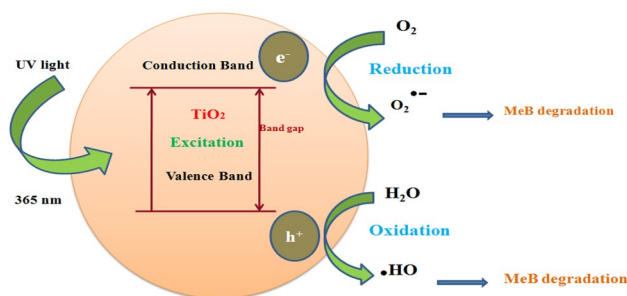


Fig. 12 Shows the degradation mechanism of TiO₂ NPs

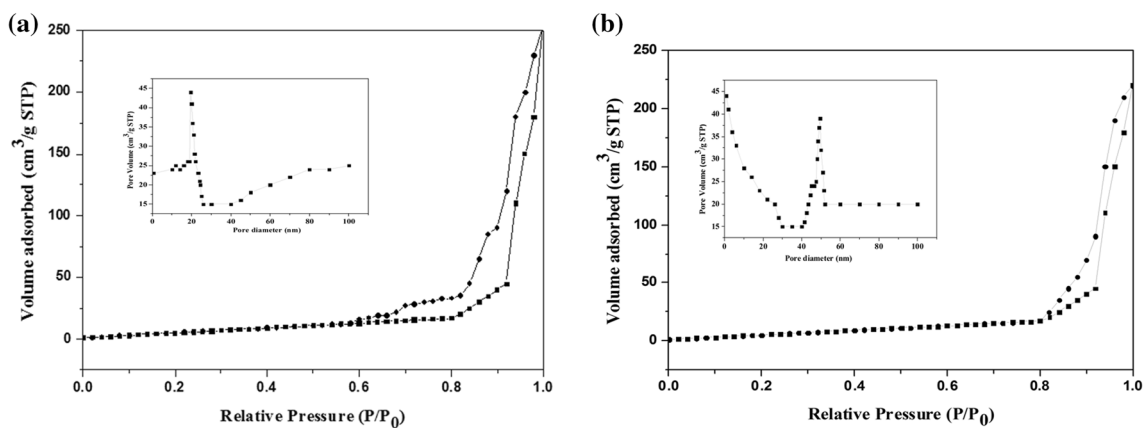


Fig. 13 a–b Shows the BET analysis of TiO₂ NPs

optical properties of optical bandgap are dependent on the calcination temperature, this was due to lower calcination temperature have high optical bandgap energy than the other calcination temperatures and it is used for optical device applications. The complete decolourization of the MeB dye was followed by UV–Visible spectrophotometry and COD method. PVP–TiO₂ NPs calcined at 500 °C exhibit better photocatalytic activity than PVP–TiO₂ NPs calcined at 700 °C. The above results are clearly indicated the importance of specific surface area in controlling the photocatalytic reactivity of PVP–TiO₂ photocatalyst. It is showed a strongly increase in the absorption of all solid samples in the UV light range regarding the reference of the PVP–TiO₂ Degussa P-25. In the present work of UV light, we showed a strong improvement especially for the PVP–TiO₂ (500 °C) compared to the reference of Degussa P-25. Therefore, it was concluded that the type, the small particle size and the separation of the charge carriers (e⁻/h⁺) have the major effect on photocatalyst activity of the catalyst in the present study.

References

- N. Masunga, G.S. Tito, R. Meijboom, *Appl. Catal. A: Gen.* **552**, 167 (2018)
- J. Mei, T. Liao, Z. Sun, *J. Energy Chem.* **27**, 127 (2018)
- A. Dey, *Mater. Sci. Eng. B.* **229**, 217 (2018)
- N. Bion, F. Can, X. Courtois, D. Duprez, *Met. Oxides Heterog. Catal.* **6**, 353 (2018)
- A.J. Haider, R. Hassan, A. Anbari, G.R. Kadhim, C.T. Salame, *Energy Proced.* **119**, 345 (2017)
- H. Cheshideh, F. Nasirpour, *J. Electroanal. Chem.* **797**, 133 (2017)
- C.B.D. Marien, T. Cottineau, D. Robert, P. Drogui, *Appl. Catal. B: Environ.* **194**, 6 (2016)
- H. Rasoulnezhad, G. Kavei, K. Ahmadi, M.R. Rahimpour, *Appl. Surf. Sci.* **408**, 10 (2017)
- L. Schlur, S.B. Colin, P. Gilliot, M. Gallart, G. Pourroy, *Mater. Sci. Eng. C* **38**, 19 (2014)
- K.D. Kumar, G.P. Kumar, K.S. Reddy, *Mater. Today Proc.* **2**, 3742 (2015)
- M. Morozova, P. Kluson, J. Krysa, M. Vesely, O. Solcova, *Proced. Eng.* **42**, 580 (2012)
- R. Singh, P. Kumari, P.D. Chavan, S. Datta, S. Dutta, *Opt. Mater.* **73**, 383 (2017)
- X. Deng, C.K. Chan, H. Tüysüz, *ACS Appl. Mater. Interfaces* **8**, 32495 (2016)
- K.R. Reddy, B.C. Sin, C.H. Yoo, W. Park, K.S. Ryu, J.S. Lee, D. Sohn, Y. Lee, *Scr. Mater.* **58**, 1013 (2008)
- Y.P. Zhang, S.H. Lee, K.R. Reddy, A.I. Gopalan, K.P. Lee, *J. Appl. Polym. Sci.* **104**, 2750 (2007)
- K.R. Reddy, K.P. Lee, A.I. Gopalan, *J. Nanosci. Nanotechnol.* **7**, 3125 (2007)
- A.M. Showkat, Y.P. Zhang, M.S. Kim, A.I. Gopalan, K.R. Reddy, K.P. Lee, *Bull. Korean Chem. Soc.* **28**, 1992 (2007)
- K.R. Reddy, K.P. Lee, A.I. Gopalan, M.S. Kim, A.M. Showkat, Y.C. Nho, *J. Polym. Sci. Part A: Polym. Chem.* **44**, 3364 (2006)
- K.R. Reddy, K. Nakata, T. Ochiai, T. Murakami, D.A. Tryk, A. Fujishima, *J. Nanosci. Nanotechnol.* **11**, 3695 (2011)
- M. Hassan, E. Haque, K.R. Reddy, A.I. Minett, J. Chenc, V.G. Gomes, *Nanoscale* **6**, 11994 (2014)
- K.R. Reddy, K.P. Lee, A.I. Gopalan, *Colloids Surf. A* **320**, 56 (2008)
- J. Hu, H. Li, S. Muhammad, Q. Wu, Q. Jiao, *J. Solid State Chem.* **253**, 120 (2017)
- M. Lian, X. Wu, Q. Wang, W. Zhang, Y. Wang, *Ceram. Int.* **43**, 9883 (2017)
- M. Rajesh, J. Raj, R. Manikandan, B.C. Kim, S.Y. Park, K.H. Yu, *Mater. Today Energy* **6**, 104 (2017)
- S. Benyakhrou, A. Belmokhtar, A. Zehhaf, A. Benyoucef, *J. Mol. Struct.* **1150**, 585 (2017)
- S. Benykhlef, A. Bekhoukh, R. Berenguer, A. Benyoucef, E. Morallon, *Colloid Polym. Sci.* **294**, 1885 (2016)
- F. Chouli, I. Radja, E. Morallon, A. Benyoucef, *Polym. Compos.* **38**, E260 (2017)
- I. Radja, H. Djelad, E. Morallon, A. Benyoucef, *Synth. Met.* **202**, 32 (2015)
- F. Chouli, A. Zehhaf, A. Benyoucef, *Macromol. Res.* **22**, 31 (2014)
- A. Gebru, C. Das, *J. Environ. Manage.* **34**, 294 (2017)
- I. Jang, K. Song, J.H. Park, M. Kim, S.G. Oh, *Mater. Lett.* **96**, 217 (2013)

32. C. Liu, W. Sun, Y. Zhuo, C. Liu, Y. Chu, J. Alloy Compd. **581**, 120 (2013)
33. D.S. Rodríguez, M. Guadalupe, M. Medrano, H. Remita, V.E. Barrios, J. Environ. Chem. Eng. **1**, 24 (2018)
34. B.B. Kadhim, Energy Proced. **119**, 722 (2017)
35. A. Rastar, M.E. Yazdanshenas, A. Rashidi, S.M. Bidoki, Arab. J. Chem. **10**, s224 (2017)
36. M.B. Askari, Z.T. Banizi, S. Soltani, M. Seifi, Opti. **157**, 239 (2018)
37. M.B. Askari, Z.T. Banizi, M. Seifi, S.B. Dehaghi, P. Veisi, Opti. **149**, 454 (2017)
38. T. Makanyire, A. Jha, S. Sutcliffe, Int. J. Miner. Process. **157**, 6 (2016)
39. M. Afuyoni, G. Nashed, I.M. Nasser, Energy Proced. **6**, 20 (2011)
40. M.R.D. Khaki, M.S. Shafeeyan, A.A.A. Raman, W.M.A.W. Daud, J. Mol. Liq. **8**, 1243 (2017)
41. Y. Yu, J. Wang, J.F. Parr, Proced. Eng. **27**, 456 (2012)
42. X. Li, S. Dong, H. Yan, C. Wu, Proced. Eng. **27**, 1491 (2012)
43. R.A. Zayadi, F.A. Bakar, J. Photochem. Photobiol. A Chem. **346**, 350 (2017)
44. G. Yan, J. Gan, J. Du, Yi, Proced. Eng. **27**, 1283 (2012)
45. T. Chen, C. Luo, D. Wang, Y. Xiong, Phys. Proced. **18**, 142 (2011)
46. D. Shaposhnik, P.E. Llobet, F.G. Guirado, X. Vilanova, Proced. Eng. **25**, 1136 (2011)
47. C.M. Firdaus, M.S.B. Shah Rizam, M. Rusop, S.R. Hidayah, Proced. Eng. **41**, 1373 (2012)
48. L. Zhang, Z. Li, X. Mou, Li, Proced. Eng. **27**, 556 (2012)
49. S. Jiang, I. Lieberwirth, K. Landfester, R. Muñoz-Espí, D. Crespy, Nanotechnology **28**, 405601 (2017)
50. K.R. Reddy, V.G. Gomes, M. Hassan, Mater. Res. Express **1**, 015012 (2014)
51. K.R. Reddy, M. Hassan, V.G. Gomes, Appl. Catal. A: Gen. **489**, 16 (2015)
52. K.R. Reddy, K. Nakata, T. Ochiai, T. Murakami, D.A. Tryk, A. Fujishima, J. Nanosci. Nanotechnol. **10**, 7957 (2010)